Journal of the European Ceramic Society 22 (2002) 2883–2892

www.elsevier.com/locate/jeurceramsoc

Sintering behavior and mechanical properties of nano-sized Cr_3C_2/Al_2O_3 composites prepared by MOCVI process

Chih-Lung Chen, Wen-Cheng J. Wei*

Department of Materials Science and Engineering, National Taiwan University, 1 Roosevelt Rd, Section 4, Taipei 106, Taiwan, ROC

Received 9 October 2001; received in revised form 15 March 2002; accepted 24 March 2002

Abstract

A process using metal-organic chemical vapor infiltration (MOCVI) conducted in fluidized bed was employed for the preparation of nano-sized ceramic composites. The Cr-species was infiltrated into Al_2O_3 granules by the pyrolysis of chromium carbonyl ($Cr(CO)_6$) at 300–450 °C. The granulated powder was pressureless sintered or hot-pressed to achieve high density. The results showed that the dominant factors influencing the Cr-carbide phases formation, either Cr_3C_2 or Cr_7C_3, in the composite powders during the sintering process were the temperature and oxygen partial pressure in the furnace. The coated Cr-phase either in agglomerated or dispersive condition was controlled by the use of colloidal dispersion. The microstructures showed that fine (20 – 600 nm) Cr_xC_y grains ($\leq$8 vol.%) located at Al_2O_3 grain boundaries hardly retarded the densification of Al_2O_3 matrix in sintering process. The tests on hardness, strength and toughness appeared that the composites with the inclusions (Cr_3C_2) had gained the advantages over those by the rule of mixture. Even 8 vol.% ultrafine inclusions have greatly improved the mechanical properties. The strengthening and toughening mechanisms of the composites were due to grain-size reduction, homogenous dispersion of hard inclusions, and crack deflection. © 2002 Published by Elsevier Science Ltd.

Keywords: Al_2O_3; Composites; Cr_3C_2; Cr_7C_3; MOCVI; Sintering behavior; Mechanical properties

1. Introduction

Ceramic matrix composites have recently come into prominence for structural applications because of their fascinating mechanical properties at room as well as higher temperature. A composite material consisting of Al_2O_3 as a matrix phase and Cr_3C_2 as the second dispersive phase was prepared by Fu and coworkers.[1–3] The composite with 10–40 vol.% Cr_3C_2 particulates demonstrated superior mechanical properties better than those of the matrix phase. Due to the high modulus of Cr_3C_2 and its outstanding high-temperature erosion resistance up to 1100 °C, Cr_3C_2-based composite has been reported ideally suitable for hot extrusion die. Furthermore, its high electrical conductivity is better than the lowest limit (10^{-2} Ω^{-1} -cm^{-1}) allowed for EDM (electrical discharge machine).[3] Those qualities make the composite more favorable for low cost applications.

A number of authors have studied the coating of metal layer by pyrolysis of metal organic precursors.[4–11] Ultrafine nano-composite powder can be synthesized from the molecular precursor by gas reaction technique. Metal-organic chemical vapor deposition (MOCVD) was developed in previous works[9–11] and successfully applied in gas-reaction processes of $Cr(CO)_6$ and $Mo(CO)_6$. Furthermore, the MOCVD process was recently applied for the infiltration of Mo-species in Al_2O_3 matrix for the preparation of nano Mo/Al_2O_3 composites.[12]

The advantages of the addition of ultrafine inclusions have been reported by Niihara and Nakahira in several aspects,[13–15] namely the reduction of grain size of the matrix grain, the strengthening, and fracture toughening advantages. In this study, a fluidized powder reactor was used for MOCVI processes. The crystalline structures of the Cr-species might show several phases, including pure-Cr, Cr_2O_3, Cr_3C_2, CrO_2, and CrCO, etc.[7–11] The addition of Cr-carbides could have homogenous Cr distribution and nano-sized inclusions in Al_2O_3 matrix. The implementation of a fluidized powder bed for the preparation of CrO_2/Cr_2O_3 nanopowder/ceramic composite powders is presented. Besides, this

* Corresponding author. Tel.: +886-2-2363-2684; fax: +886-2-2363-4562.

E-mail address: wjwei@ccms.ntu.edu.tw (W.-C.J. Wei).

0955-2219/02/$ - see front matter © 2002 Published by Elsevier Science Ltd.
PII: S0955-2219(02)00058-4

study also used colloidal process to prepare well-dispersed Cr_3C_2/Al_2O_3 mixture before sintering. A small amount (<8 vol.%) of Cr_3C_2 inclusions is enough to significantly improve the strength of the composites.

2. Experimental

2.1. Powder and sample preparation

Chromium hexacarbonyl ($Cr(CO)_6$, 99.7%, Alta Aesar, Johnson Matthey Company, USA) was used as a source powder. The carbonyl vapor was carried by N_2 gas (99.9% pure) into the fluidized powder reactor for MOCVI process.[12] Based on Lander's results, $Cr(CO)_6$ evaporates readily at ambient temperature under vacuum with a saturation pressure P:[4]

$$\log P = 11.832 - 3755.2/T \quad (1)$$

where T is the reaction temperature in Kelvin. The calculated saturation pressure of the carbonyl is 10 Torr at 75 °C. The source chamber was maintained at a constant temperature (75 °C) under vacuum (10 Torr) using a water bath. A schematic diagram of the apparatus is shown in Fig. 1. The fluidization column made of quartz, had an inside diameter of 75 mm and a length of 500 mm. The pressure drop in the column was measured with a pressure sensor located between the top and bottom of the column. A rotary vacuum pump (R.P.) was installed with cold trap systems. Besides, there was a vacuum gauge (G) to detect the pressure in front of the pump. The temperature inside the powder bed was measured with a thermocouple. The temperature controller (T.C.) connected to an electrical heating system allowed the operation to maintain a constant temperature in the hot-wall reactor.

Because the temperature in the reactor dominated the reactions and the saturation pressure of the carbonyl species, the resulted microstructure and characteristic of Cr-products were greatly affected. One of the parameters is the yield of the Cr-species by MOCVI process. Precursor would evaporate and partially deposit on the wall of reactors to cause various yields. Yield (Y) of Cr-product was evaluated from the following relationship:

$$Y = \frac{W_{f1} - W_{f0}}{W_{S1} - W_{S0}} \quad (2)$$

where W_{f1} and W_{f0} represent the mass of infiltrated composite and alumina powders, respectively, and W_{S1} and W_{S0} is the mass of $Cr(CO)_6$ precursor and the remainder after gas reaction.

The carbonyl vapor flowed through the lowest part of the fluidized powder bed and infiltrated into or deposited on fluidizing alumina agglomerates[1] (AKP-50, Sumitomo Chemical Co., Tokyo, Japan) in a N_2 stream, as shown in Fig. 1. The deposited agglomerates was analyzed by XRD and showed a $Cr_2O_3/CrO_2/Al_2O_3$ mixture. Then, the mixture ($Cr_2O_3/CrO_2/Al_2O_3$) was put in aqueous solution with 1.0 mass% dispersant (Darvan C, Vanderbilt Co., Norwalk, USA) based on

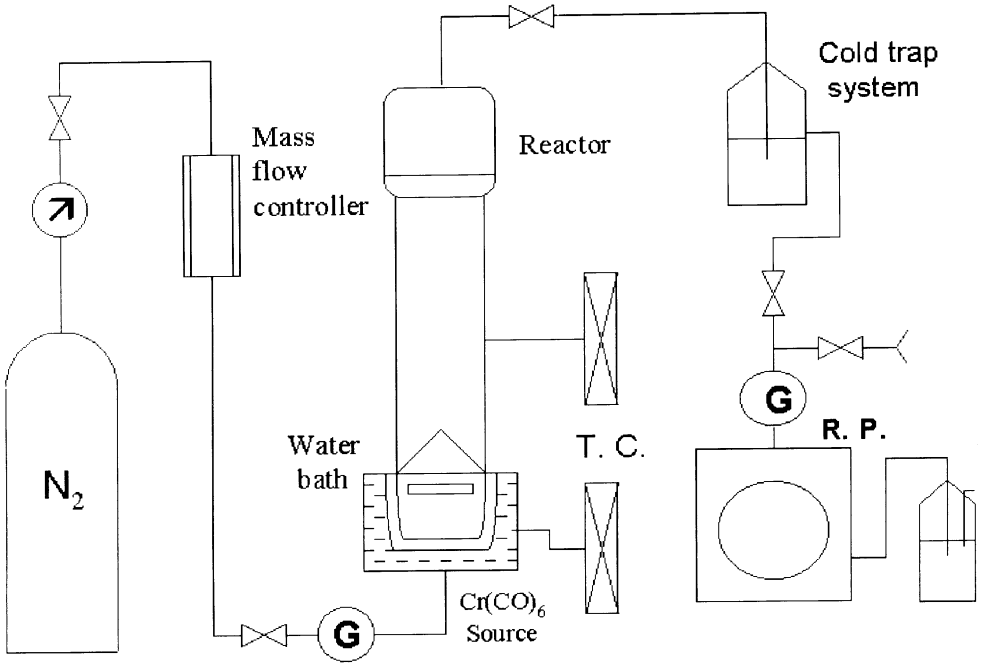

Fig. 1. Schematic diagram of the fluidized powder reactor and equipments for MOCVI.

[1] The Al_2O_3 before coating was pre-heated in a dry oven at 105°C overnight.

powder and ball-milled for 24 h. The well-dispersed suspension with 30 vol.% powder loading was pressure-casting by an air pressure of 10 kg/cm^2 (980 kPa) to form a green compact. After drying, the compact was ground and sieved through a 150-mesh screen for hot-pressing, or made ready for pressureless sintering.

2.2. Densification

Either pressureless sintering or hot-pressing methods were applied for the densification of powder mixture. The 150 mesh mixtures were die-pressed at first, then put into a BN-coated graphite die and hot-pressed at a pressure of 25 MPa for 1 h in a HP furnace (High-multi 5000, Fujidempa Kogyo Co., LTD, Japan) at 1400 °C under vacuum (5×10^{-4} Torr). The pressureless sintering were conducted at temperatures between 1100 and 1600 °C.

2.3. Characterization of properties

2.3.1. Analyses of phases and microstructure observation

The phases of sintered composites were identified by an X-ray diffractometer (Philips PW1710, Philips Co., Netherlands). The morphologies of polished and fractured surfaces of composites were analyzed by scanning electron microscopy (SEM, Philips XL30, Philips Co., USA) equipped with an X-ray energy dispersive spectroscopy (EDS, DX-4, EDAX Co., USA). The TEM samples were cut to thin layers by Isomet (Buehler Ltd., USA) and a 3 mm diameter disc was prepared by using an ultrasonic disc cutter (model 601, Gatan Co., USA). The thickness of the sample was ground and reduced to <100 μm by using Minimet polisher (Buehler Ltd., USA). Afterward, the sample was dimpled to a thickness of <25 μm by a dimple grinder (model 656, Gatan Co., USA) and ion milled by an ion miller (Gatan Co., USA). The transmission electron microscopes (TEM, 100CXII, Jeol Co., or Hitachi Model HF-2000 FETEM, Japan) were employed to observe the microstructure of the sample previously coated with a thin carbon layer.

2.3.2. Thermal shrinkage analysis

The sintering behaviors and shrinkage of the composites were tested by a thermal mechanical analyzer (TMA, SETSYS TMA16/18, SETARAM Co., France). The operation conditions were conducted usually from room temperature to 1400 °C under vacuum condition with a heating rate of 10 °C/min.

2.3.3. Mechanical tests

The sintered or HP composite disks were cut and ground to the dimensions of $3\times4\times35$ mm^3. All surfaces of the test bars were polished with various diamond pastes with sizes from 30, 6 to 1 μm. The flexural strength was conducted following a four-point bending test method according to ASTM C1161 standard. Hardness and toughness were measured by a Vickers indentor (AKASHl, AVK-A, Japan). The toughness values were calculated following the equation proposed by Evans.[16] These mechanical properties were measured at room temperature.

3. Results and discussion

3.1. Effects of temperature and atmosphere

The yield of $Cr(CO)_6$ decomposition at various reaction temperatures in a N_2 flow rate of 1.5 l/m and a constant pressure of 10 Torr is shown in Fig. 2. The yield increases with the reaction temperature, and reaches a maximum at 400 °C. When the reaction temperature is 400 °C during the MOCVI process, the highest conversion ratio shows 60% yield. The residual products are lost by two ways. Part of the residue was adhered on the wall of fluidization column and the rest was sucked away by the mechanical pump. The Cr-species were stuck on the cold trap tubes during the MOCVI process.

The deposited composites were analyzed by XRD. A series of the spectra of the composites treated in vacuum (5×10^{-2} Torr) is shown in Fig. 3. At low temperature, i.e. 600°C, the spectra show that Cr_2O_3 phase is the as-deposited Cr-species. According to our previous analysis,[11] a few per cent of carbon can form a solid solution in the oxide. At higher temperature, Cr_3C_2 appears above 700°C, but it is replaced by Cr_7C_3 above 1100°C. The formation of the carbides from Cr_2O_3 in reducing atmosphere can be:

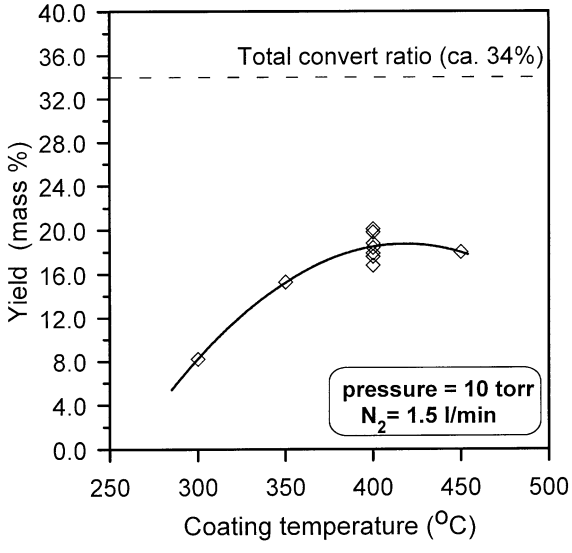

Fig. 2. Plot of the decomposition yield of $Cr(CO)_6$ at various coating temperatures and at a constant pressure of 10 Torr.

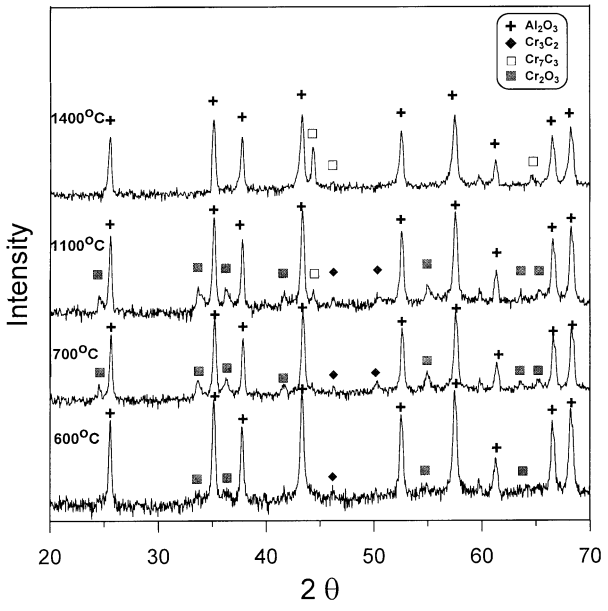

Fig. 3. XRD patterns of Cr_7C_3/Al_2O_3 composites heated at different temperatures for 1 h in vacuum condition.

$$3/2Cr_2O_{3(S)}+2CO_{(g)}= Cr_3C_{2(S)} + 13/4O_{2(g)}$$
$$\Delta G = 1800765 + 234.9T \quad (3)$$

The Cr_3C_2 (orthorhombic phase) likely transforms into Cr_2O_3 in the O_2-rich atmosphere. The above reaction was proven by XRD analysis.

There are several Cr-carbide phases in Cr–C system, such as Cr_3C_2, Cr_7C_3 and $Cr_{23}C_6$. The Cr_3C_2 is unstable in O_2-rich atmosphere compared to the others. It is easily oxidized at high temperature and even at very low partial pressure of oxygen in accordance with the thermodynamic results, suggesting the following oxidation reaction of Cr_3C_2:

$$Cr_3C_{2(S)}+5/14O_{2(g)}= 3/7Cr_7C_{3(S)}+5/7CO_{(g)}$$
$$\Delta G= -63284.7-66.78T \quad (4)$$

and the carbon and oxygen reaction in graphite furnace can be

$$C_{(S)}+1/2O_{2(g)}= CO_{(g)} \quad \Delta G= -111700-87.65T \quad (5)$$

By means of Eqs. (4) and (5), we can draw an Ellingham diagram as shown in Fig. 4 which shows the variation of the Gibbs free energy with temperature at 1 atm. The Gibbs free energy of $CO_{(g)}$ formation (−258 kJ/mol) is lower than that of $Cr_7C_{3(S)}$ formation (−175 kJ/mol) at 1400°C. Because of the heating element, the insulation and mold in the furnace were made of graphite, the graphite easily reacts with oxygen if it is an impurity in flowing $N_{2(g)}$, to form $CO_{(g)}$ during HP

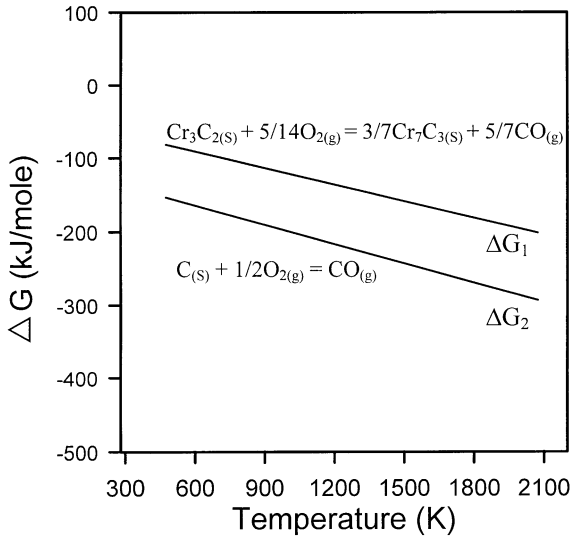

Fig. 4. Free energy versus temperatures of two oxidation reactions. Note that $CO_{(g)}$ is more stable than $Cr_7C_{3(s)}$ in an oxygen-containing atmosphere.

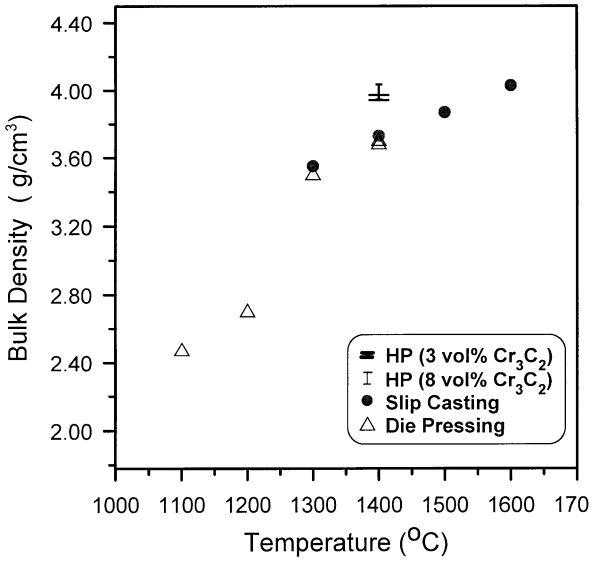

Fig. 5. Bulk densities of Cr-carbide PL sintered and HP at various temperatues for 1 h in vacuum condition of 5×10^{-2} Torr (PL) or 5×10^{-4} Torr (HP). The green density of the composites was 2.07 g/cm^3, the density of HPed Al_2O_3 was 3.86 g/cm^3.

sintering at 5×10^{-4} Torr. In other words, the CO gas is more stable than Cr_7C_3 in oxygen-contained atmosphere. Besides, Eq. (4) can be confirmed by the appearance of Cr-carbide samples which turn to a purple color (i.e. Cr_7C_3). The formation of Cr_3C_2 during HP (hot-pressing) at a vacuum condition of 5×10^{-4} Torr is easily differentiated from the formation of Cr_7C_3 during pressureless sintering at a poor vacuum condition of 5×10^{-2} Torr. The Cr_3C_2 will react with oxygen gas and form Cr_2O_3 or Cr_7C_3 in a poor vacuum condition. Moreover, a high-density matrix will restrict the CO producing diffusing out from the interior of matrix.

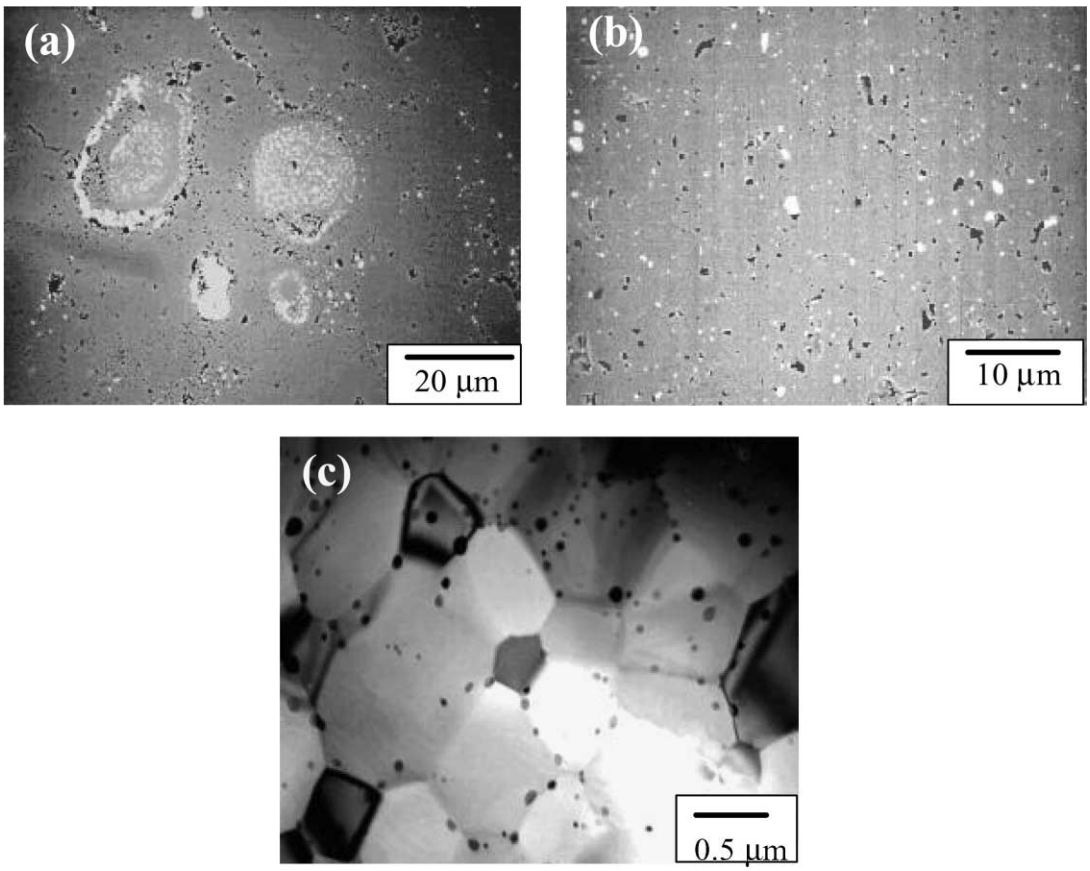

Fig. 6. SEM and TEM of Cr_7C_3/Al_2O_3 composites (a) as-prepared by MOCVI, (b) and (c) followed by colloidal processing. The sintering conditions were PL sintered at 1600 °C for 1 h in vacuum. Note that Cr_7C_3 phase was formed in those sintering conditions.

As a result, the interior of the densified sample shows a mixture of Cr_3C_2/Al_2O_3 phases.

Fig. 5 shows bulk densities of several sintered composites. The initial stage of shrinkage obviously occurs above 1200 °C. Although the product phases are different,[2] colloidal process in association with PL sintering or HP can indeed get density (4.03 g/cm^3) very close to the theoretical density (T.D.) of the composite. Besides, by means of the high pressure bearing on the composite during sintering can reach the final density at 1400 °C, either with 3 or 8 vol.% Cr_3C_2. The final density of hot pressed 3 vol.% Cr_3C_2/Al_2O_3 composite is similar to that of 8 vol.% Cr_3C_2/Al_2O_3 composite.

3.2. Microstructural development and sintering behavior

A small amount of hard agglomerates which are larger than 20 μm may exist if without colloidal dispersion, as shown in Fig. 6(a). In order to improve the homogeneity of Cr-carbide dispersion, dispersing, ball milling, and slip casting techniques were adapted. The average grain size of Cr-carbide in sintered composite is below 1.0 μm and the phase is well dispersed within the Al_2O_3 matrix [Fig. 6(b)]. The agglomerated or micron-sized carbide grains in colloidal-processed composites are hardly observed in the matrix [Figs. 6(b) and 7(a)]. The TEM micrographs [Figs. 6(c) and 7(b)] appear that Cr-carbide grains may have the sizes as small as 20 nm. Most of the intergranular Cr_7C_3 and Cr_3C_2 grains are larger than 50 nm, and the intragranular Cr_7C_3 and Cr_3C_2 grains are in the range of 20 ± 10 nm and are spherical in shape. Only a few Cr-carbide inclusions are larger than 1 μm [Figs. 6(b) and 7(a)].

The size of Al_2O_3 matrix grains in the composites is smaller with the addition of Cr_3C_2. The size of most Al_2O_3 grains is restrained to less than 1.2 μm, essentially predicted by the following equation, which relates the matrix grain size (G) to the volume fraction (f) of the second phases, and the grain size (r) of inclusions:

$$G = K_t \frac{r}{(\varphi_p f)^{1/3}} \quad (6)$$

where K_t is a constant, φ_p is the volume fraction of inclusions which is able to restrain the motion of matrix grain boundaries. The topological relation emphasizes the strong pinning effect of a second phases to the matrix grain. Nevertheless, ultra-fine inclusions are

[2] The theoretical density (T.D.) of Cr_3C_2 and Cr_7C_3 is 6.92 and 6.68 g/cm^3, respectively.

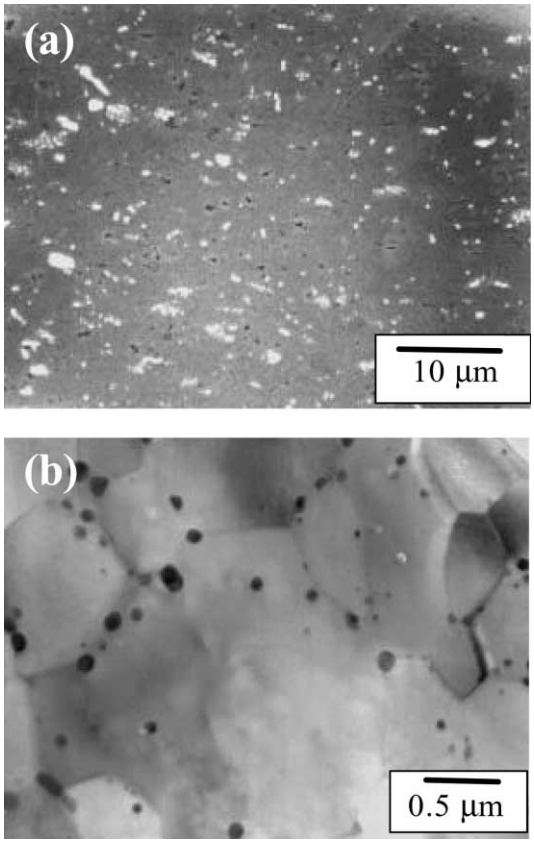

Fig. 7. (a) SEM and (b) TEM micrograph of granular 8 vol.% Cr_3C_2/Al_2O_3 composites prepared by colloidal processing. The samples were HP at 1400 °C in 1 h in vacuum. Note that Cr_3C_2 phase was formed.

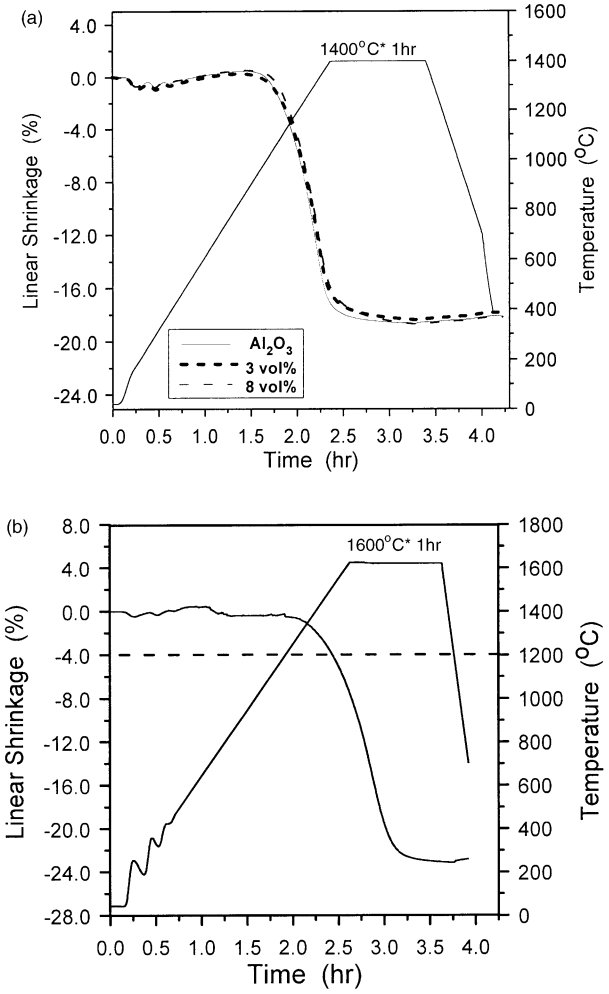

Fig. 8. Dilatometric curves showing the shrinkage behaviours of two composites: (a) sintering of die-pressed powder mixture at 1400 °C; (b) sintering of colloidal-processed powder mixture at 1600 °C for 1 h in vacuum condition.

unable to be observed in Al_2O_3 matrix due to the resolution of SEM. But these carbide grains can be clearly observed by TEM. Ultra-fine, nano-sized Cr-carbide can be fabricated by the gas reaction process.

Several studies reported the sintering behavior and phase transformation during the process of Cr_3C_2/Al_2O_3 composite at high temperature.[1,2,18,19] Most of their results showed that the relative density and flexural strength of Cr_3C_2/Al_2O_3 sintered in vacuum were better than that of argon. Besides, it was proven in previous research that the phase stability of Cr_3C_2 phase was quite sensitive to the temperature and sintering environment.

The die-pressed pure Al_2O_3, 3 vol.% Cr-carbide/Al_2O_3, and 8 vol.% Cr-carbide/Al_2O_3 were examined by TMA in vacuum condition. The results are shown in Fig. 8(a). All three curves start to shrink at ca. 900 °C, and show maximal densification rate at ca. 1300 °C. Total 18% linear shrinkage is resulted after holding at 1400 °C for 1 h. The pure Al_2O_3 was densified nearly identical to that of Cr-carbide composites. But the sintering temperature of the composites for full densification is higher than that of pure Al_2O_3 which needs temperatures $\geqslant$1500 °C for 1 h. There are two reasons for this. One is the impeding effect of Al_2O_3 grains by the inclusions. The other is the back-stress that results from the difference of sintering rate between the carbide phase and Al_2O_3 matrix.

The linear shrinkage of colloidal-processed 8 vol.% Cr-carbide/Al_2O_3 composite sintered at 1600 °C for 1 h is about 23.5% [Fig. 8(b)] which is larger than that sintered at 1400 °C. The bulk density of the 8 vol.% Cr-composite can reach 4.03 g/cm^3 if PL sintered at 1600 °C (Fig. 5).

3.3. Mechanical properties

It is expected that the hardness of Al_2O_3 will increase by the addition of Cr_3C_2 inclusions because the hardness of Cr_3C_2 (27 GPa) is much higher than the hardness 18.6 GPa of pure Al_2O_3. The Vickers hardness of the composites is shown in Fig. 9(a) as a function of inclusion content. The data represent the measured values of 6–8 specimens. The standard deviation is also shown in the figure. Based on the Soroka's study,[20] the

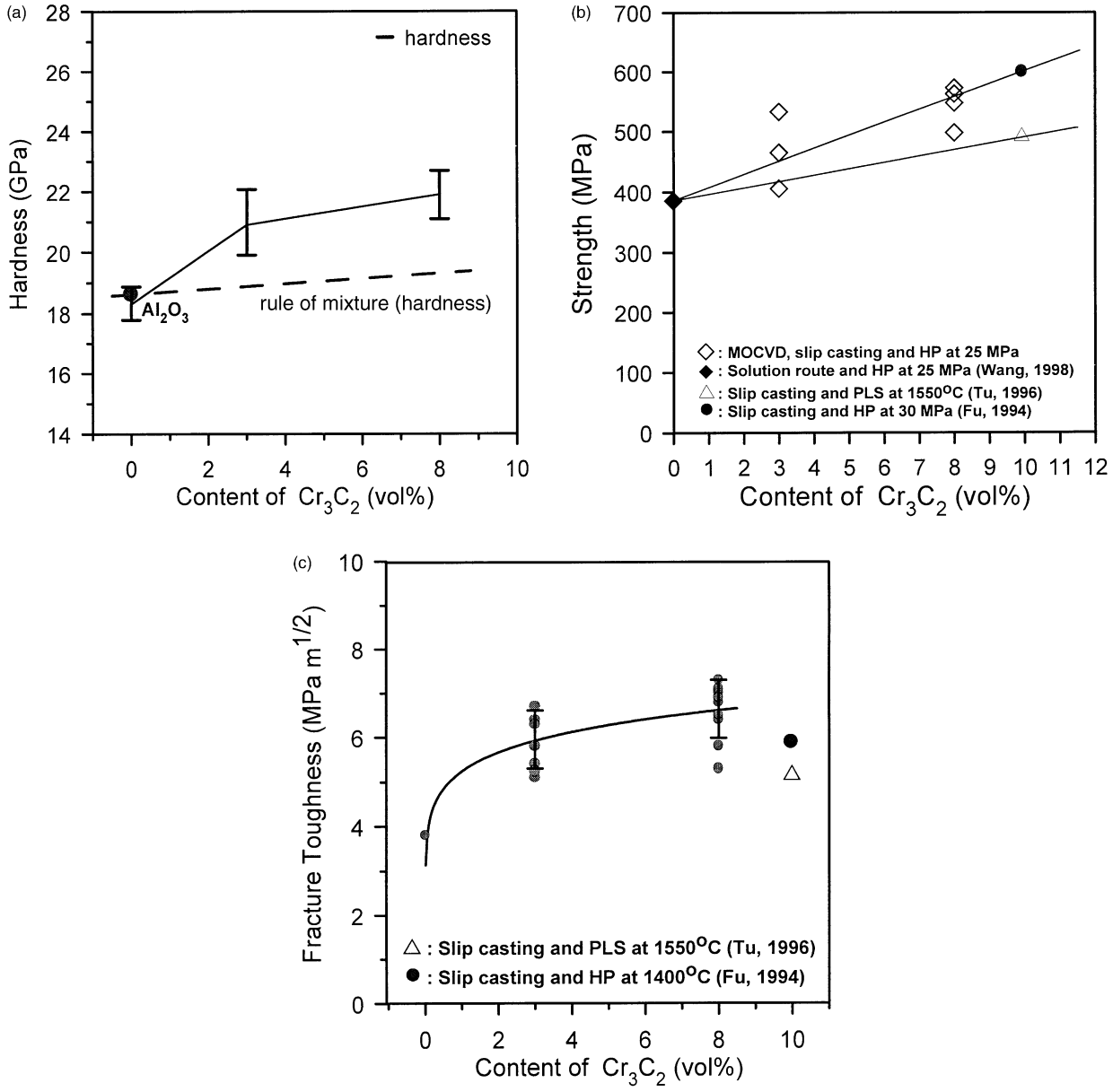

Fig. 9. (a) Vickers hardness, (b) four-point bending strength, and (c) fracture toughness of Cr_3C_2/Al_2O_3 composite plotted against content of Cr_3C_2. The composites were hot-pressed at 1400 °C for 1 h in vacuum.

more the porosity, the smaller the hardness of ceramic materials. The influence of porosity to hardness was neglected in this investigation. First, a Cr_3C_2/Al_2O_3 composite was fabricated by colloidal processing and hot-pressing. We consider that the composite has reached its final densification. The dotted line in Fig. 9(a) means the hardness plotted according to the rule of mixture. The hardness of the composites is indeed greater than the values calculated by the rule of mixture.

Fig. 9(b) shows the four-point flexural strength of Al_2O_3-based composites as a function of Cr_3C_2 content. Obviously, the flexural strengths of 3 and 8 vol.% Cr_3C_2 composites are improved from 380 MPa of pure Al_2O_3 to 600 MPa. The strength increases with increasing Cr_3C_2 content, and shows a maximal value of 546 MPa of 8 vol.% Cr_3C_2 composite. The strength shows 44% improvement with the addition of 8 vol.% Cr_3C_2. Based on the Petch relation,[21] the finer the grain sizes, the better the strength of materials. This relation suggests that an increasing amount of Cr_3C_2 could further reduce the size of Al_2O_3 matrix, thus improving the strength of the composite. More important, the Cr_3C_2 was synthesized and colloidal processed to achieve a well-dispersive condition. Therefore, the flexural strength is optimized by means of the uniform distribution of the fine Cr_3C_2 inclusions.

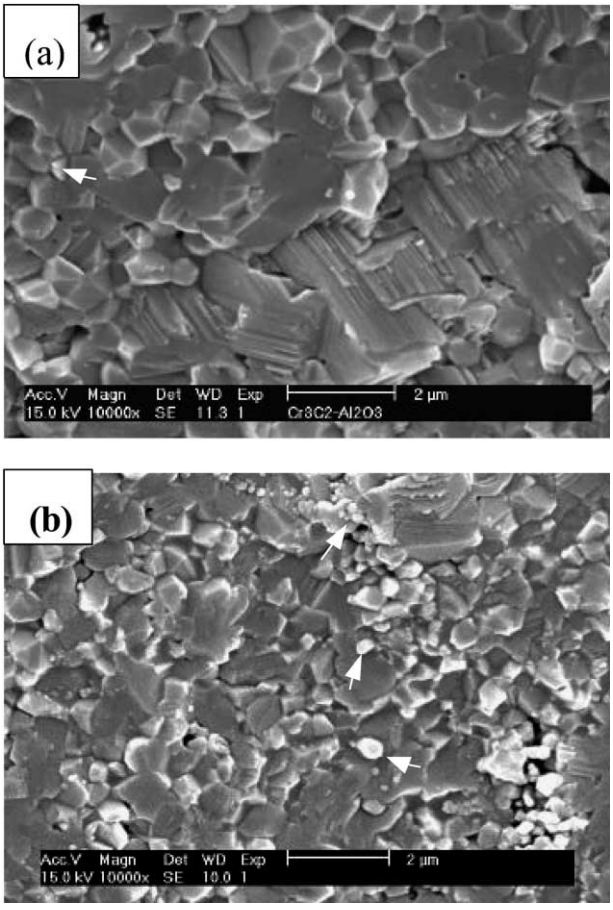

Fig. 10. SEM micrographs of the fracture surfaces of Cr_3C_2/Al_2O_3 composites with (a) 3 vol.% Cr_3C_2, or (b) 8 vol.% Cr_3C_2 content. Cr-phase is indicated by arrows in the figure.

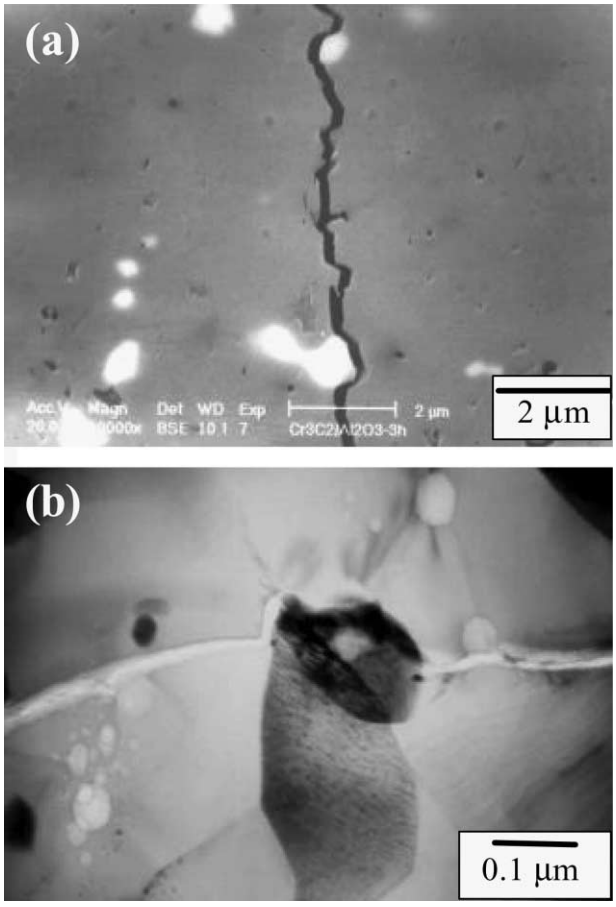

Fig. 11. (a) SEM (back scattering image) and (b) TEM micrographs of the interaction of inclusions with crack formed by Vickers indentation on Cr_3C_2/Al_2O_3 composites. The samples were HP at 1400 °C for 1 h in vacuum.

The toughness of the Cr_3C_2/Al_2O_3 composites is illustrated in Fig. 9(c). The toughness of the composites increases with increasing inclusion content. The average value of toughness of 3 and 8 vol.% Cr_3C_2 composites are 5.8 and 6.3 MPa $m^{1/2}$, respectively.

The SEM morphologies of the fracture surfaces of Cr_3C_2/Al_2O_3 composites are shown in Fig. 10. Fine inclusions pointed out in Fig. 10(b) show sphere shape and have Cr_3C_2 composition as confirmed by EDS analysis. The fracture mode of the Al_2O_3 and 3 vol.% Cr-composites apparently exhibit a mixture of transgranular and intergranular modes. However, the samples with large grains show higher possibility of transgranular fracture mode, and intergranular fracture on smaller grains.

The transgranular fracture seems to happen along the slip plane of Al_2O_3, as shown in the right-hand corner of Fig. 10(a). The stepwise cleavage features shown on the surface of larger Al_2O_3 grains is as conspicuous as the occurrence of transgranular fracture. Since the transgranular fracture greatly depends upon the matrix grain size and the contents of Cr_3C_2 inclusions, the 8 vol.% Cr_3C_2 composites show more intergranular fracture, and should have better toughening behavior than that of pure Al_2O_3 and 3 vol.% Cr_3C_2 composite.

Besides, residual stresses may exist on the interface between Cr_3C_2 and Al_2O_3. The mismatch of CTE ($\Delta\alpha = 2.8\times10^{-6}/°C$) during the cooling process may result in a tensile force in the matrix along the radial direction and a compressive force along the tangential direction. The larger the inclusion, the greater the stresses. If a crack is approaching the inclusion, the analysis shows that the crack will be deflected thus leading to an increase of the fracture surface area. With regard to the toughening mechanism, one microstructure of the crack/inclusion interaction induced by the Vicker's indentation is revealed in Fig. 11. A significant feature is observed that the crack propagated along the particle/matrix interfaces. The crack pattern apparently reveals that the primary toughening mechanism is crack deflection. Based on Evans' model of crack deflection,[22] the toughness increases is mainly due to the increase of total fracture surface area and the change of the fracture mode. Accordingly, the toughness increases as the

crack-tip region is subjected to the local compressive stress to decrease the stress intensity while the cracks are propagating within the Al_2O_3 matrix. The crack deflection through the nearest particles induced by residual thermal tension is effectively caused by accounting the number of inclusions available on the crack paths. We believe that 8 vol.% of ultra-fine Cr_3C_2 inclusions can lead to appropriate crack deflection in Al_2O_3, thereby improving the toughness of the composites.

Nevertheless, there are no other conspicuous toughening effects in the composite reinforced by ultra-fine ($\leqslant 50$ nm) Cr_3C_2 inclusion. One TEM observation shown in Fig. 11(b) indicates that the crack does not propagate straightly in Al_2O_3 matrix, but rather around the Cr_3C_2 inclusion, as pointed out in Fig. 11(b). That means that even a small Cr_3C_2 inclusions also have a toughening effect in Al_2O_3 matrix.

4. Conclusion

Nano-sized Cr_3C_2 on Al_2O_3 granules were synthesized by MOCVI. A maximum deposition yield of 60% is obtained at the optimal deposition temperature 400 °C. Well-dispersed inclusions (Cr_3C_2 or Cr_7C_3) either in agglomeration or dispersive condition in the Al_2O_3 matrix can be controlled.

The sintering temperature and oxygen partial pressure are the dominant and sensitive factors which affect the phase transformation of Cr-carbide during sintering process. The dense Cr_3C_2/Al_2O_3 composite can be prepared by hot-pressing sintered at 1400 °C for 1 h at 25 MPa in vacuum. Otherwise, Cr_7C_3/Al_2O_3 composites can be obtained in poor vacuum condition. Besides, the shrinkage behaviors between pure Al_2O_3 and low ($\leqslant 8$ vol.%) Cr-carbide composites are hardly differentiated.

Based on the microstructural observation, the intergranular and intragranular Cr-carbide grains are larger than 50 nm and in the sizes of 20 nm, respectively. The Al_2O_3 matrix grains can be controlled to sizes less than 1.2 μm. Two effects were introduced by the fine particles in the composites, less constrain of densification and greater inhibition of matrix grain growth. However, the microstructure of the composite has significantly influenced the mechanical properties. The strength and toughness of Al_2O_3 can be improved by the addition of 8 vol.% Cr_3C_2 hard inclusions. Grain size reduction and homogenous distribution of the inclusions in the Al_2O_3 matrix are the primary strengthening mechanisms. In addition, the major toughening mechanism for Cr_3C_2/Al_2O_3 composite generated by fine Cr_3C_2 particles is crack deflection. The hardness and strength improvement of the composites are similar, and show up to 44% increase. On the other hand, the contribution of toughness by 8 vol.% Cr_3C_2 is nearly 40%.

Uncited reference

Ref 17 is not cited in the text

Acknowledgements

The authors like to thank the research funding supported by National Science Council in Taiwan (NSC89–2216-E-002–001) and helpful discussion with Dr. C.M. Wu in CSIST.

References

1. Fu, C. T., Li, A. K. and Wu, J. M., Microstructure and mechanical properties of Cr_3C_2 particulate reinforced Al_2O_3 matrix composites on microstructure and mechanical properties. *J. Mater. Sci*., 1993, **28**, 6285–6294.
2. Fu, C. T., Li, A. K. and Wu, J. M., Effects of post-sinter hot isostatic pressing processes on microstructures and mechanical properties of Al_2O_3-Cr_3C_2 composites. *Br. Cerm. Trans*, 1994, **93**, 178–182.
3. Shu, K. M., Fu, C. T. and Liu, J. M., Electrodischarge-machining of Al_2O_3/Cr_3C_2 composites. *J. Mater. Sci. Lett*., 1994, **13**, 1146–1148.
4. Lander, J. J. and Germer, L. H., Plating molybdenum, tungsten, and chromium by thermal decomposition of their carbonyls. *American Institute Mining Metal Tech*., 1947, **14**(6), 1–42.
5. Okada, N., Katsumura, Y. and Ishigure, K., Improvement of corrosion resistance of carbon steel using chemical vapor deposition from the mixture of $Mo(Co)_6$ and $Cr(CO)_6$ with an ArF-excimer laser. *Appl. Phys*., 1994, **A58**, 99–105.
6. Singmaster, K. A., Houle, F. A. and Wilson, R. J., Photochemical deposition of thin film from the metal hexacarbonyls. *J. Phys. Chem*., 1990, **94**, 6864–6875.
7. Perkins, F. K., Hwang, C. and Onellion, M., Chromium oxide films fabricated by $Cr(CO)_6$ chemical vapor deposition. *The Solid Films*, 1991, **198**, 317–329.
8. Okada, N., Katsumura, Y. and Ishigure, K., Improvement of corrosion resistance of carbon steel using chemical vapor deposition from the mixture of $Mo(Co)_6$ and $Cr(CO)_6$ with an ArF-excimer laser. *Appl. Phys*., 1994, **A58**, 99–105.
9. Maruyama, T. and Akagi, H., Chromium oxide thin film prepared by chemical vapor deposition from chromium acetylacetonate and chromiumhexacarbonyl. *J. Electrochem Soc*., 1996, **143**(6), 1955–1958.
10. Lo, M. H. and Wei, W. C. J., Analysis of (Cr,Mo) oxycarbide films grown on stainless steel via metallorganic chemical vapor deposition. *J. Am. Ceram. Soc*., 1997, **80**(4), 886–892.
11. Lo, M. H. and. and Wei, W. J., Processing and properties of (Cr,Mo) oxycarbides from MOCVD. *Appl. Organometal. Chem*., 1998, **12**, 1–20.
12. Lin, C. J., Young, T. and Wei, W. J., Processing and microstructure of nano-Mo/Al_2O_3 composites from MOCVD and fluidized bed. *Nanostructured Materials*, 1999, **11**(8), 1361–1377.
13. Sekino, T., Nakajima, T. and Niihara, K., Mechanical and magnetic properties of nickel dispersed alumina-based nanocomposite. *Materials Letters*, 1996, **29**, 165–169.
14. Nakahira, A. and Niihara, K., Sintering behavior and consolidation process for Al_2O_3/SiC nanocomposites. *J. Ceram. Soc. Jpn*, 1992, **100**(4), 448–453.

15. Niihara, K., Nakahira, A. and Sekino, T., New nanocomposite structural ceramics. *Mater. Res. Symp. Proc*, 1993, **286**, 405–412.
16. Evans, A. G. and Charles, E. A., Fracture toughness determinations by indentation. *J. Am. Ceram. Soc.*, 1976, **59**(7–8), 371–372.
17. Huseh, C. H., Sintering behavior of powder compacts with multiherogeneities. *J. Mater. Sci.*, 1986, **21**, 2067–2072.
18. Tu, G. J., *Study on Mechanical Properties and Microstructure of Pressureless-sintered Al_2O_3/ Cr_3C_2 Composite*. Thesis for Master Degree, NCKU, Taiwan, 1995.
19. Huang, J. J., *Injection Molding of Cr_3C_2/Al_2O_3 Composites*. Thesis for Master Degree, NCKU, Taiwan, 1995.
20. Soroka, J. and Sereda, J., Interrelation of hardness, modulus of elasticity and porosity in various gypsum systems. *J. Am. Ceram. Soc.*, 1968, **5**(6), 337.
21. Petch, N. J., Cleavage strength of polycrystals. *J. Iron and Steel Inst. (London)*, 1953, **174**(1), 25–28.
22. Evans, A. G. and Faber, K. T., Toughening of ceramics by circumferential microcracking. *J. Am. Ceram. Soc.*, 1981, **64**(7), 394–398.